Chiral spin-wave excitations of the spin-$\frac{5}{2}$ trimers in the langasite compound $Ba_3NbFe_3Si_2O_{14}$

Jens Jensen
Niels Bohr Institute, Universitetsparken 5, DK-2100 Copenhagen, Denmark
(Received 6 June 2011; revised manuscript received 10 August 2011; published 2 September 2011)

The inelastic scattering of neutrons from magnetic excitations in the antiferromagnetic phase of the langasite compound $Ba_3NbFe_3Si_2O_{14}$ is analyzed theoretically. In the calculations presented, the strongly coupled spin-$\frac{5}{2}$ Fe triangles are accounted for as trimerized units. The weaker interactions between the trimers are included within the mean field and random phase approximations. The theory is compared with linear spin-wave theory, and a model is developed that leads to good agreement with the published results from unpolarized and polarized neutron-scattering experiments.

DOI: 10.1103/PhysRevB.84.104405 PACS number(s): 75.30.Ds, 75.10.−b, 75.25.−j

I. INTRODUCTION

The langasite compound $Ba_3NbFe_3Si_2O_{14}$ belongs to the space group $P321$ (space group number 150), where triangles of Fe^{3+} ($L=0$, $S=5/2$) ions are placed in a lattice as indicated in Figs. 1 and 2. The space group contains no improper symmetry elements and the other ions may be arranged in two different mirrored ways as specified by the sign of the structural chirality factor $\epsilon_T = \pm 1$. The Hamiltonian for the $S=5/2$ spins of the Fe ions is assumed to be

$$\mathcal{H} = \frac{1}{2}\sum_{i,\xi}\sum_{j,\eta} J_{\xi\eta}(ij)\,\mathbf{S}_\xi(i)\cdot\mathbf{S}_\eta(j) + \sum_i \mathcal{H}_T(i), \qquad (1)$$

where i and j are the triangle numbers, and ξ and $\eta = 1,2,3$ denote the different spins in each triangle, as defined in Fig. 1. The Hamiltonian for the isolated triangles is determined in terms of the intratriangle interaction $J_1 > 0$ and an anisotropy term assumed to be a Dzyaloshinsky-Moriya (DM) interaction:

$$\begin{aligned}\mathcal{H}_T &= J_1(\mathbf{S}_1\cdot\mathbf{S}_2 + \mathbf{S}_2\cdot\mathbf{S}_3 + \mathbf{S}_3\cdot\mathbf{S}_1)\\ &\quad + D_c(\mathbf{S}_1\times\mathbf{S}_2 + \mathbf{S}_2\times\mathbf{S}_3 + \mathbf{S}_3\times\mathbf{S}_1)\cdot\hat{\mathbf{c}}. \qquad (2)\end{aligned}$$

The system is antiferromagnetically ordered below $T_N = 27$ K.[1,2] The moments are confined to lie in the ab plane, the property of which is in accordance with the anisotropy introduced in Eq. (2) (independent of the sign of D_c). All triangles in a certain ab plane are identical, and the three spins $\langle\mathbf{S}_1^i\rangle$, $\langle\mathbf{S}_2^i\rangle$, and $\langle\mathbf{S}_3^i\rangle$ in the ith triangle are making an angle of $\gamma = \epsilon_\gamma(2\pi/3)$ with each other so that $\langle\mathbf{S}_1^i\rangle + \langle\mathbf{S}_2^i\rangle + \langle\mathbf{S}_3^i\rangle = \mathbf{0}$, where $\epsilon_\gamma = \pm 1$ defined in Fig. 1 denotes the two possible orientations of the ordered spin triangles. The moments along a line parallel to the c axis rotate the angle $\phi = \mathbf{Q}\cdot\mathbf{c} \cong \epsilon_H(2\pi/7)$ from one layer to the next along the c axis, where $\epsilon_H = \pm 1$ denotes the helicity (chirality) of the helically ordered moments.

The magnetic excitations at low temperatures in the helically ordered phase have been studied experimentally by two independent groups: Stock *et al.*[3] determined the dispersion relations of the spin waves propagating in the a^*c^* plane from inelastic scattering of unpolarized neutrons, whereas Loire *et al.*[4] investigated the excitations by doing inelastic scattering experiments in the b^*c^* plane with both unpolarized and polarized neutrons. Loire *et al.*[4] carried through a linear spin-wave analysis of their results from which they concluded that the moments were all ordered in right-handed helices, corresponding to $\epsilon_H = +1$, in the $\epsilon_T = -1$ enantiopure crystal they were investigating.

The spin system in $Ba_3NbFe_3Si_2O_{14}$ is relatively strongly frustrated, and the validity of the mean field (MF) and the random phase approximation (RPA), on which the linear spin-wave theory is based, may be questioned. The dominant cause for frustration is the strong interaction J_1 between the three spins in the Fe triangles. In this paper, I have improved the theoretical description of the system by treating the spin triangles as trimerized units placed in a mean field due to the interactions between neighboring trimers. The properties of the trimers are determined accurately by a numerical diagonalization of the mean-field trimer Hamiltonian, and the corresponding spectrum of collective trimer excitations is calculated by the use of standard RPA numerical techniques.[5,6] Before the numerical analysis is presented in Sec. III, it is instructive to consider the approximate but analytical behavior of the spin system as done in Sec. II. The spin-wave theory applied in this section is not the standard one based on the Holstein-Primakoff transformation, but it is straightforward to show that the present RPA approach and the standard spin-wave theory are equivalent to leading order (see, for instance, Ref. 5). In Sec. IV, the cross section for polarized neutrons is calculated numerically, and the results are compared with the experimental results obtained by Loire *et al.*[4] The conclusions are presented in Sec. V.

II. LINEAR SPIN-WAVE THEORY

A coordinate system is assigned to each spin, defined so that the local z axis is along the direction of the ordered spin, and the y axis is along the c axis and common for all coordinate systems. In the spin-wave limit at $T=0$, where the spins are fully polarized, the ground state of the ith triangle is $|000\rangle$. The states are defined by $S_{\xi z}|n_1n_2n_3\rangle = (S-n_\xi)|n_1n_2n_3\rangle$, where $\xi = 1,2,3$. The interactions between the different triangles lead to a mean field acting only on the z components (neglecting any anisotropy within the ab plane)

$$\mathcal{H}_{\rm MF} = -h(S_{1z} + S_{2z} + S_{3z}) + \mathcal{H}_T\,. \qquad (3)$$

In this section, it is assumed that $h \gg J_1$ and only terms to first order in J_1/h and D_c/h are included. The intratriangle

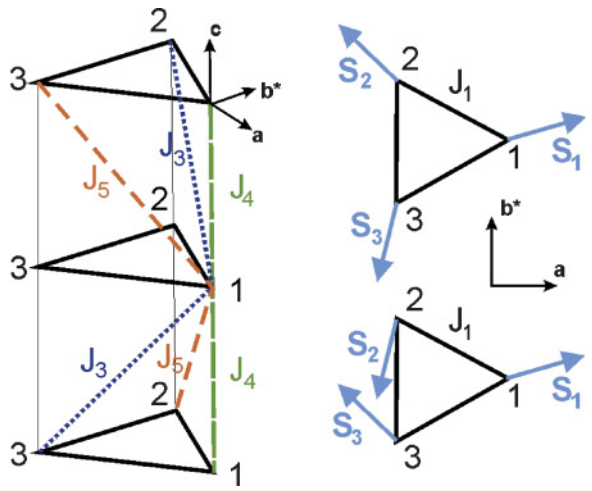

FIG. 1. (Color online) Fe triangles are stacked on top of each other along the c axis in the $Ba_3NbFe_3Si_2O_{14}$ crystal. The line parallel to the c axis through the center of the triangles is a threefold symmetry axis, and the three altitudes of one triangle are twofold symmetry axes. The oxygen ions are placed in different positions along the paths determining the interplanar exchange constants J_3, J_4, and J_5. The shortest super-superexchange path (and bond angles closest to π) defines (Ref. 1) the structural chirality $\epsilon_T = \pm 1$. If this path is the one determining J_5 as defined in the figure, the corresponding chirality would be $\epsilon_T = -1$, whereas $\epsilon_T = +1$ if this path is the one leading to the exchange interaction J_3. The right part of the figure shows the ordered spins in one of the triangles, where the moments rotate the angle $\gamma = \epsilon_\gamma(2\pi/3)$ for increasing site index. The upper triangle shows the case where $\epsilon_\gamma = +1$, whereas the orientation of the ordered spins in the lower triangle corresponds to $\epsilon_\gamma = -1$.

interactions imply that the ground state $|g\rangle$ is modified into

$$|g\rangle = |000\rangle + \lambda(|110\rangle + |101\rangle + |011\rangle),$$
$$\lambda = \frac{3SJ_1 - 2SD_c \sin\gamma}{8h}. \tag{4}$$

The first-order modification of the ground state does not affect the ground-state energy to leading order, and it is

$$E(g) = -3Sh - \tfrac{3}{2}S^2 J_1 + 3S^2 D_c \sin\gamma. \tag{5}$$

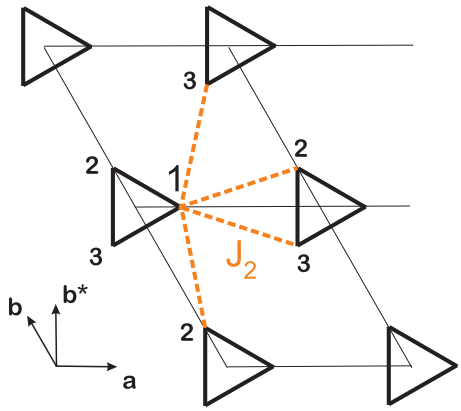

FIG. 2. (Color online) The triangles within an ab plane with a definition of the exchange parameter J_2.

The presence of the DM anisotropy implies a specific sign for γ. The product $D_c \sin\gamma$ has to be negative, and the orientation of the ordered spin triangles is determined by the sign of D_c according to $\epsilon_\gamma = -\text{sign}(D_c)$.

The thermal expectation value $\langle S_{\xi z}\rangle = \langle g|S_{\xi z}|g\rangle = S - \mathcal{O}(\lambda^2)$ and, by neglecting the second-order modification, the exchange field is determined from the interaction parameters defined in Figs. 1 and 2 as

$$h = -2S[\,2J_2\cos\gamma + J_4\cos\phi + J_3\cos(\phi+\gamma) + J_5\cos(\phi-\gamma)]. \tag{6}$$

ϕ is the angle of rotation of $\mathbf{S}_\alpha$ within the plane, when going from one ab plane to the next in the positive c direction. The value of ϕ is found by maximizing h (minimizing the ground-state energy) and is determined by

$$\tan\phi = R\sin\gamma, \quad R = \frac{2(J_5 - J_3)}{2J_4 - J_3 - J_5}. \tag{7}$$

It is remarkable that a difference between J_3 and J_5 implies that ϕ becomes nonzero with no need for an interaction between next-nearest-neighboring spins along the c axis. Experimentally,[2] it is found that $|\phi|$ is close to $2\pi/7$. The relation also shows that the magnetic helicity and the orientation of the ordered spin triangles are intimately related, that is,

$$\epsilon_H = \text{sign}(R)\,\epsilon_\gamma. \tag{8}$$

The three lowest excited states are (approximately)

$$|a\rangle = (|100\rangle + w|010\rangle + w^2|001\rangle)/\sqrt{3},$$
$$|b\rangle = (|100\rangle + w^2|010\rangle + w|001\rangle)/\sqrt{3}, \tag{9}$$
$$|c\rangle = (|100\rangle + |010\rangle + |001\rangle)/\sqrt{3},$$

where $w = e^{i2\pi/3}$. The corresponding excitation energies $\Delta_\alpha = E(\alpha) - E(g)$ are

$$\Delta_a = \Delta_b = h + \tfrac{3}{4}SJ_1 - \tfrac{5}{2}SD_c\sin\gamma,$$
$$\Delta_c = h + \tfrac{3}{2}SJ_1 - SD_c\sin\gamma. \tag{10}$$

The collective excitations of this system may be derived by introducing the "bosonlike" (creation) operators for the ith triangle: $\alpha_i^+|g\rangle = |\alpha\rangle$, where $\alpha = a, b$, or c. By neglecting the interactions between the triangles and introducing the Fourier transforms of the operators, the single-trimer MF Hamiltonian may be written as

$$\mathcal{H}_{\text{MF}} = E(g) + \frac{1}{N}\sum[\Delta_a a_{\mathbf{q}}^+ a_{\mathbf{q}} + \Delta_b b_{\mathbf{q}}^+ b_{\mathbf{q}} + \Delta_c c_{\mathbf{q}}^+ c_{\mathbf{q}}]. \tag{11}$$

Within the subspace of the four lowest spin states for the ith triangle, we may write

$$S_{1x} = \left[m_x^c(c_i^+ + c_i) + m_x^a(a_i^+ + a_i + b_i^+ + b_i)\right]\sqrt{\frac{S}{6}},$$
$$S_{1y} = i\left[m_y^c(c_i^+ - c_i) + m_y^a(a_i^+ - a_i + b_i^+ - b_i)\right]\sqrt{\frac{S}{6}}, \tag{12}$$

and similarly for the other spin components, except that the (a_i, b_i^+) and (a_i^+, b_i) terms are multiplied, respectively, by w

and w^2 in the expressions for the spin components of $\mathbf{S}_2$, and by w^2 and w in the spin components of $\mathbf{S}_3$. To first order in J_1/h, the relative matrix elements are

$$\begin{aligned} m_x^c &= 1+2\lambda, \quad & m_y^c &= 1-2\lambda, \\ m_x^a &= 1-\lambda, \quad & m_y^a &= 1+\lambda\,, \end{aligned} \tag{13}$$

in terms of the mixing parameter λ defined in (4). The next step is to substitute these expressions for the spin components in the exchange Hamiltonian, which leads to an effective Hamiltonian quadratic in the excitations operators. By introducing the Fourier transforms of the operators, the Hamiltonian stays diagonal with respect to the $(c_{\mathbf{q}},c_{\mathbf{q}}^+)$ operators, when $\mathbf{q}$ is parallel to the c axis. We shall concentrate on this case in the following, i.e., that $\mathbf{q}\cdot\mathbf{c} = qc$. In the zero-temperature limit, the only nonzero commutator relations are $[\alpha_{\mathbf{q}},\alpha_{\mathbf{q}'}^+] \approx \delta_{\mathbf{q}\mathbf{q}'}$, where $\alpha = a$, b, or c. From the equations of motion, the energy squared of the c-mode excitations propagating along the c axis is then found to be

$$\begin{aligned} E_c^2(q) = &\left(\Delta_c + S\left(m_x^c\right)^2\{[J(Q)+2J_2]\cos(qc)-2J_2\}\right) \\ &\times\left(\Delta_c + S\left(m_y^c\right)^2\{[J(0)-4J_2]\cos(qc)+4J_2\}\right), \end{aligned} \tag{14}$$

where the two exchange parameters are

$$\begin{aligned} J(Q) &= 2[J_4\cos\phi + J_3\cos(\phi+\gamma) + J_5\cos(\phi-\gamma) - J_2], \\ J(0) &= 2[2J_2 + J_3 + J_4 + J_5]. \end{aligned} \tag{15}$$

$J(Q)$ is also the parameter determining the exchange field $h = -\langle S_{\xi z}\rangle J(Q)$. The remaining part of the excitation Hamiltonian leads to two w modes with mixed $|a\rangle$ and $|b\rangle$ state characters, and the squared energies of these modes are

$$\begin{aligned} E_{w1}^2(q) &= \left[\Delta_a + S\left(m_x^a\right)^2 J_x(q)\right]\left[\Delta_a + S\left(m_y^a\right)^2 J_y(q)\right], \\ E_{w2}^2(q) &= \left[\Delta_a + S\left(m_x^a\right)^2 J_x(-q)\right]\left[\Delta_a + S\left(m_y^a\right)^2 J_y(-q)\right], \end{aligned} \tag{16}$$

where

$$\begin{aligned} J_x(q) &= 2J_4\cos\phi\cos(qc) + 2J_3\cos(\phi+\gamma)\cos(qc+\gamma) \\ &\quad + 2J_5\cos(\phi-\gamma)\cos(qc-\gamma) + J_2, \\ J_y(q) &= 2J_4\cos(qc) + 2J_3\cos(qc+\gamma) \\ &\quad + 2J_5\cos(qc-\gamma) - 2J_2. \end{aligned} \tag{17}$$

In general, $J_{x,y}(-q) \neq J_{x,y}(q)$, which means that the two modes are not symmetric around $q = 0$, and instead we have that $E_{w1}(q) = E_{w2}(-q)$.

Introducing the expressions for Δ_α and the relative matrix elements into Eqs. (14) and (16), the squared excitations energies are, to leading order in λ,

$$\begin{aligned} E_c^2(q) = &S^2[1-\cos(qc)][-J(Q)-2J_2] \\ &\times[3J_1 - 2D_c\sin\gamma - J(Q) \\ &+ 4J_2 + \{J(0)-4J_2\}\cos(qc)] \end{aligned} \tag{18}$$

and

$$\begin{aligned} E_w^2(q) = &S^2[J_y(q) - J(Q) - 2D_c\sin\gamma] \\ &\times\left[\tfrac{3}{2}J_1 - 3D_c\sin\gamma + J_x(q) - J(Q)\right]. \end{aligned} \tag{19}$$

Equation (18) shows that the energy of the c mode $E_c(q)$ vanishes linearly with q, when $q \to 0$. This Goldstone mode, which appears because the rotational symmetry in spin space around the c axis is broken in the ordered phase, reflects that it costs no energy to rotate the ordered structure around the c axis. In the case of a c excitation propagating along the c axis, all the c components of the spins in a certain ab plane are moving in phase, whereas the w modes imply that the plane of the spins in a certain triangle is oscillating out of the ab plane, and this oscillation is affected by the DM anisotropy. Because of this anisotropy, the w modes show an energy gap at $q = \pm Q$:

$$E_w(Q) \simeq S(-D_c\sin\gamma\{3J_1 + 2J_x(\phi/c) - 2J(Q)\})^{1/2}. \tag{20}$$

The transverse (x,y) components of the spins are defined in a coordinate system for which the x axis rotates the angle ϕ around the y or c axis from one ab plane to the next. In a neutron experiment with the scattering vector $\mathbf{k}$ along the c axis, modulo a reciprocal lattice vector, the excitations detected are those described above at $q = k$, when the scattering derives from the y or c component of the spins. If the scattering is instead due to the x component, the experiment detects the excitations at $q = k + Q$ and $q = k - Q$. The c mode behaves similarly to the spin waves in a simple helix, where the c component reflects the branch for which the Goldstone mode starts out from $k = 0$, whereas an ab scattering vector component reflects the two branches, where the Goldstone modes emerge from the two magnetic Bragg peaks at $k = \pm Q$. The situation is different for the w modes. The excitations detected by the c component are those determined above at $q = k$, i.e., a $w1/w2$ mode emerging (subjected to a small gap) from the Bragg point at $+Q$ and a $w2/w1$ mode emerging from the other Bragg point at $-Q$. When the w modes are detected via the component in the ab plane, the wave numbers of the c-component branches are translated by Q or $-Q$. Two of those become pseudo-Goldstone modes starting out from $k = 0$, whereas the two other branches are placed with their starting points at $k = 2Q$ and $-2Q$. The intensities of the extra $\pm 2Q$ branches are, however, always going to be weak.

Although the c mode shows similarities with the spin waves in a simple helix, there is one important difference, namely, that the cross section of the c mode vanishes when the total scattering vector is parallel to the c axis. In this case, the excitations are detected exclusively via the spin components perpendicular to the c axis. For the c modes propagating along the c axis, all the locally defined spin components within one ab plane oscillate in phase, and this means that the sum of the ab components for a spin triangle stays zero during the c-mode oscillations. The two w branches starting out from $\pm 2Q$ have no cross section either, which leaves the two pseudo-Goldstone w branches starting out from $k = 0$ to be the only ones appearing in a scan along $(0\,0\,q)$. Such a scan would, effectively, only show a single spin-wave branch (see Fig. 7 in the next section), in strong contrast to that expected in the case of a simple helically ordered system. In general, $J_y(q) = J_y(2\phi/c - q)$, whereas $J_x(q) \neq J_x(2\phi/c - q)$, which means that there are actually two branches in the plot along $(0\,0\,q)$ shown in Fig. 7, but the energy difference is small, about 0.06 meV at maximum around $q = 1.25$.

In addition to the DM anisotropy included in Eq. (3), the symmetry of the system also allows the following term[7]:

$$D_{ab}(\hat{\mathbf{r}}_{12}\cdot\mathbf{S}_1\times\mathbf{S}_2+\hat{\mathbf{r}}_{23}\cdot\mathbf{S}_2\times\mathbf{S}_3+\hat{\mathbf{r}}_{31}\cdot\mathbf{S}_3\times\mathbf{S}_1), \quad (21)$$

but this interaction does not affect any of the quantities considered above to leading order in D_{ab}/h. The numerical analysis presented below shows that this coupling may weakly perturb the ordered structure by inducing a small oscillating c component on top of the spiraling ordered moments lying in the ab plane. The ordered c components have a constant magnitude within an ab plane, the magnitude of which varies sinusoidally along the c axis with the same period as the helix. Using a D_{ab} with the same magnitude as $D_c = 0.0038$ meV considered in the next section, the scattering intensity due to the oscillating c-axis moment is found to be a factor of 10^6 smaller than the intensity due to the a or b component. Hence, we may safely neglect any influences from D_{ab}. Finally, I may add that the simple anisotropy term $D_z(S_{1z}^2+S_{1z}^2+S_{1z}^2)$, with $D_z \simeq 0.005$ meV, may replace D_c in the explanation for the confinement of the moments to the ab plane and for the presence of the energy gap $E_w(Q)$. In contrast to the DM term, the D_z anisotropy would affect the susceptibility components in the paramagnetic phase, but the value of D_z indicated by the energy gap $E_w(Q)$ is too small to make any observable difference. However, this interaction has no influence on the choice of sign for γ, and is therefore unable to explain why the system prefers one of the two choices as found experimentally.[1]

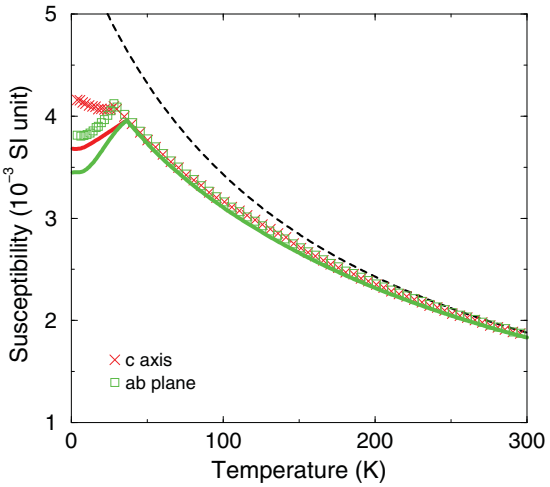

FIG. 3. (Color online) The calculated susceptibility components as functions of temperature compared with the experimental results of Marty *et al.* (Ref. 8). The red line and the red crosses denote, respectively, calculated and experimental results, when the field is applied along the c axis. The green symbols denote the results obtained when the field is applied perpendicular to the c axis. The dashed line shows the MF behavior for the corresponding simple $S = 5/2$ system. The difference between the dashed and solid lines indicates the importance of correlation between the three spins in the triangle clusters.

III. NUMERICAL MODEL CALCULATIONS

In the numerical analysis, the cluster MF Hamiltonian (3), with the self-consistent condition that $h = -\langle S_{\xi z}\rangle J(Q)$, is diagonalized precisely, and the excitation spectra are calculated without making any further approximations than the basic random phase approximation (see Refs. 5 and 6). The best MF/RPA trimer model obtained from fitting the susceptibility and the excitation data obtained by Stock *et al.*[3] is (in units of meV)

$$\begin{aligned} &J_1 = 1.25, \quad J_2 = 0.2, \quad J_3 = 0.1, \\ &J_4 = 0.064, \quad J_5 = 0.29, \quad D_c = 0.0038. \end{aligned} \quad (22)$$

The anisotropy is very small, and I have chosen the sign to be positive. This means that $\gamma = -2\pi/3$, and introducing the exchange parameter given above into the equilibrium condition (7) leads to $\tan\phi = 1.257$ or $\phi = 2\pi/7$.

The calculated results for the susceptibility components as functions of temperature are compared with experiments in Fig. 3. The dashed line in this figure shows the MF susceptibility for the same model given by (22), but with the intratriangle interaction J_1 included as a mean-field contribution. This simple MF model leads to a Néel temperature that is 70.1 K, whereas the present cluster-MF model predicts $T_N = 36.7$ K in reasonable agreement with the experimental value $T_N = 27$ K. The calculated Curie temperature is $\theta = -190$ K, and the one derived from the experimental paramagnetic susceptibility in Fig. 3 is $\theta = -188$ K (using the data within the whole interval between T_N and 300 K), hence, the experimental frustration factor $f = -\theta/T_N$ (Ref. 9) is about 7 for this system. Because of the relatively strong intratriangle interaction J_1, the system is frustrated, which invalidates the simple MF approximation. Within the cluster-MF approximation, the spin triangles are treated as correlated units, implying that the main source for frustration J_1 is accounted for in an exact way. The results above and the comparison in Fig. 3 show that the MF method is substantially improved when choosing the basis to be the spin triangles instead of the individual spins.

The parameters given by (22) lead to an exchange interaction $J(Q) = -0.821$ meV. The self-consistent diagonalization of the cluster-MF Hamiltonian in (3) with $h = -\langle S_{\xi z}\rangle J(Q)$ predicts the moment $\langle g\mu_B S_{\xi z}\rangle$ to be 4.71 μ_B/Fe in the zero-temperature limit. The moment is reduced from its fully polarized value of 5 μ_B/Fe because $|000\rangle$ is not an eigenstate for the J_1 part of the Hamiltonian (3). By introducing the model parameters in the expression (4) for the mixing parameter, the result turns out to be $\lambda = 0.57$. Hence, λ is not small compared to 1, and the approximate expressions for the spin-wave energies given by (18) and (19) would not be expected to apply. Nevertheless, the analytic spin-wave theory leads to useful results both when applying directly the final results [Eqs. (18) and (19)] or when using instead the correct cluster-MF values for the energy differences and matrix elements in the expressions (14) and (16), as shown, respectively, by the dashed and the solid lines in Fig. 4. The numerical diagonalization of (1) predicts $\Delta_a = 3.486$ meV and $\Delta_c = 4.751$ meV, and the relative matrix elements are found to be $m_x^c = 1.520$, $m_y^c = 0.618$, $m_x^a = 0.655$, and $m_y^a = 1.275$. The dispersion relations along the c axis shown in Fig. 4 have been calculated when introducing these values in the spin-wave expressions (14) and (16). The results are

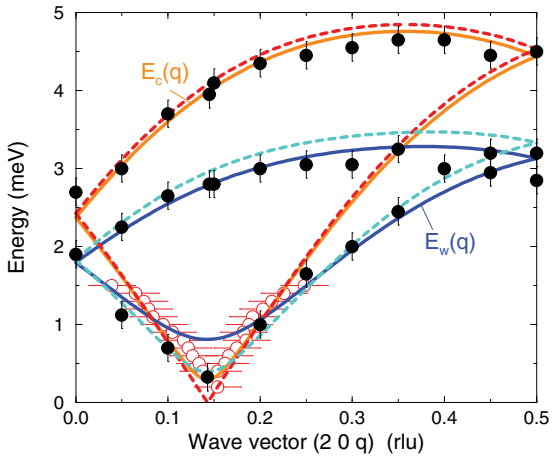

FIG. 4. (Color online) The calculated spin-wave dispersion relations along the c axis compared with the experimental results obtained at 2.5 K by Stock *et al.* (Ref. 3) along $(2\,0\,q)$. The calculated energies of the two w modes and the two branches of the c mode are shown by, respectively, the blue and orange lines, and the spectrum includes only the two times two branches observed in the experiments. The solid lines show the results obtained when introducing the calculated values of the energy splittings and the matrix elements in Eqs. (14) and (16), whereas the dashed lines are the results obtained using the linear spin-wave expressions (18) and (19).

in good agreement with experiments and with the scattering intensity maxima obtained numerically. The only difference between the numerical RPA calculations (see below) and the spin-wave results given by Eqs. (14) and (16) and shown by the solid lines in Fig. 6 is that the simplified model neglects the possible influences of the higher-lying MF levels. This minor inaccuracy is the reason why the calculated c mode shows a small energy gap at Q and that $E_w(Q)$ is too large in comparison with the numerical RPA result. The analytical spin-wave theory is valuable not because it is nearly able to reproduce the numerical results, but because it allows a precise interpretation of the numerical RPA calculations. It is possible to extend the analytic theory to cases where the wave vector also has a component in the ab plane. This is a more complex situation because all three levels are being mixed with each other.[10] The most important change is that J_2 in the spin-wave energies is being replaced by $J_2[\cos(\mathbf{q}\cdot\mathbf{a})+\cos(\mathbf{q}\cdot\mathbf{b})+\cos(\mathbf{q}\cdot\mathbf{a}+\mathbf{q}\cdot\mathbf{b})]/3$. I have not found it necessary to carry through these more demanding calculations, and neither have I tried to work out the analytical results for the spin-wave scattering intensities because all these extra complications are handled in a satisfactory and more accurate way by the numerical RPA calculations.

The numerical RPA results derived for the spin-wave scattering intensities are presented in Figs. 5 and 6. In all the calculations, the intensity variations due to the magnetic form factor of the Fe ions are neglected. The calculations of the logarithmic intensities are done with a narrow resolution (a Lorentzian with $\Gamma = 0.05$ meV), whereas a Gaussian resolution width and an intensity scale factor have been used as fitting parameters in the direct comparisons shown in Fig. 6. The two fitting parameters are the same for all the results shown by the blue lines, and both parameters have been increased by 20% in the results shown by the red lines in the right part of Fig. 6. These calculated results are compared with the experimental cross sections obtained by Stock *et al.*[3]

As discussed in the preceding section, a scan along $(0\,0\,q)$ should show only two nearly degenerate w branches starting out from the crystallographic Bragg point at $q = 1$ (in reciprocal lattice units) with the energy $E_w(Q)$, and the calculated scattering intensities obtained for such a scan are shown in Fig. 7. Preliminary measurements by Stock *et al.*[11] are consistent with this prediction. The structural parameters determined by Marty *et al.*[1] show that the distance d between the ions in the Fe triangles is very close to be equal to $(\sqrt{3}/4)\,a$ and, thereby, that $a^*d = \pi$. This means that the structure factor of the spin triangles is unchanged if $4\mathbf{a}^*$ or $4\mathbf{b}^*$ is added to the scattering vector. Hence, when neglecting any form-factor effects, the only difference between a $(0\,0\,q)$ and

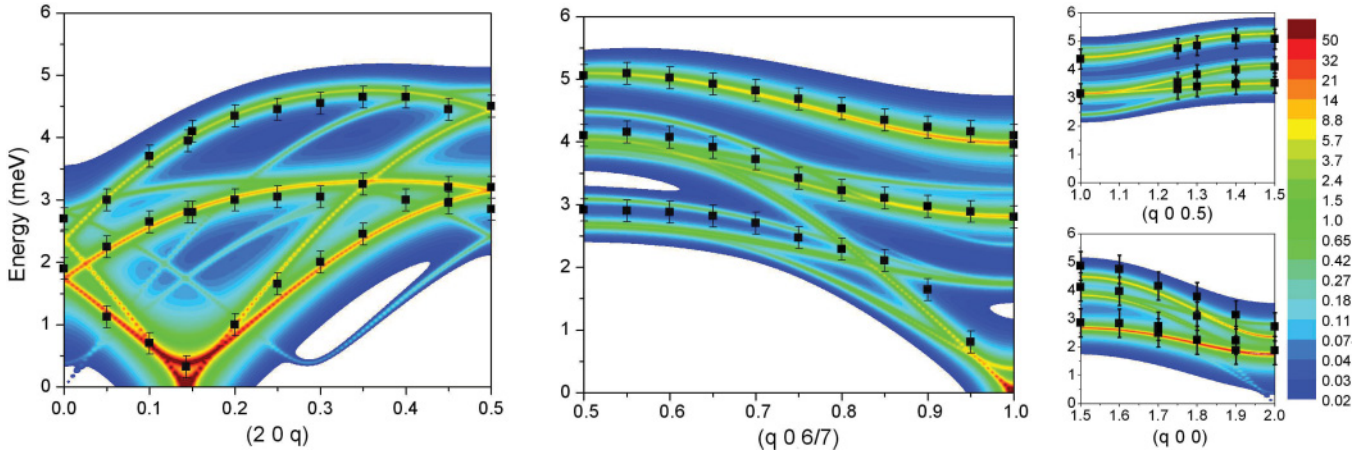

FIG. 5. (Color online) Logarithmic contour plots of the calculated spin-wave scattering intensities along different scattering vectors in reciprocal lattice units. The black squares indicate the experimental energies determined at $T = 2.5$ K by Stock *et al.* (Ref. 3). The logarithmic scale shown to the right is common for all three cases shown here and also applies to Fig. 7 and to the left figure in Fig. 8. The use of the logarithmic scale may be slightly misleading in the sense that the low-intensity branches (light green and light blue), which are easily identified in these plots, are probably not visible under realistic circumstances.

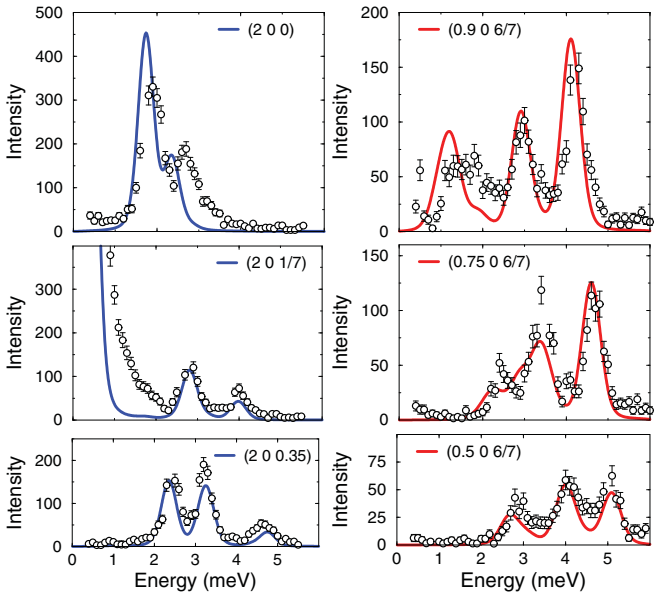

FIG. 6. (Color online) Detail comparisons between the experimental (Ref. 3) and calculated cross sections for a selection of the scattering vectors considered in Fig. 5.

a $(4\,0\,q)/(0\,4\,q)$ scan is that scattering due to the c-axis spin components, which cancels out in a $(0\,0\,q)$ scan, contributes at $(4\,0\,q)/(0\,4\,q)$. A scan along $(4\,0\,q)$ or $(0\,4\,q)$ is expected to show not only the two w modes, but also the c mode, all starting out from $q = 1$ as illustrated by Fig. 7. The w modes starting out from the magnetic Bragg point do (nearly) not appear in this scan because the total c component of the spin triangles is zero for these modes. The experimental results shown in the figure are the same as those presented in Fig. 5, but now translated so that they all fall on the two branches seen in this scan. The energy gap of the w modes, appearing in this plot at $q = 1$, has been determined in the neutron-scattering experiments by Stock *et al.*[3] and by Loire *et al.*[4] to lie between

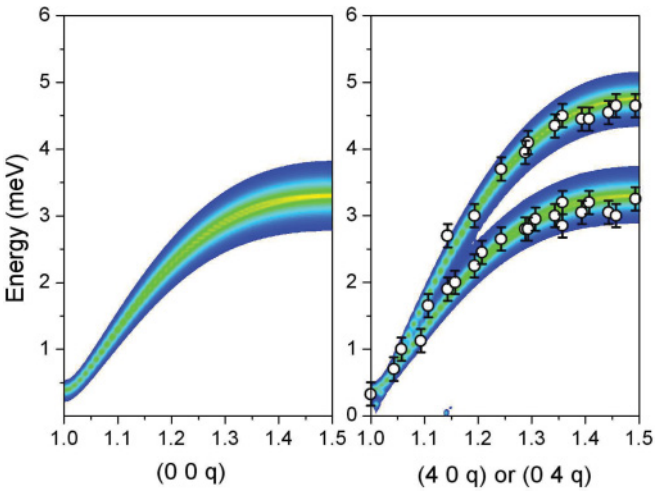

FIG. 7. (Color online) The logarithmic scattering intensities calculated along $(0\,0\,q)$ and $(4\,0\,q)/(0\,4\,q)$. The experimental results included in the $(4\,0\,q)/(0\,4\,q)$ figure are the same as those appearing in Fig. 5 and obtained by Stock *et al.* (Ref. 3), but the results have been translated by wave vectors $(0\,0\,\ell \pm Q)$.

0.35 and 0.4 meV. This value of the gap is here used for determining the numerical value of D_c. This way of plotting the experimental results also shows that the energy of the c mode at $(4\,0\,1 + Q)$, the upper peak in the $(2\,0\,0)$ scan shown in Fig. 6, is distinctively higher than the value suggested by a sinusoidal interpolation of the other c-mode results. The difference might be caused by special effects related to this particular wave vector $(2\,0\,0)$, or it may be an indication of a weak interaction between spins in next-nearest-neighboring layers. The fit to the two dispersion relations may be improved by including a ferromagnetic interaction $J_{12}(2c) \cong -0.01$ meV (between sublattice 1 and 2 at a distance of $2c$ along the c axis), however, the improvements are not really significant and this possible modification is abandoned.

The experiments of Stock *et al.*[3] were all performed in the a^*c^* plane, whereas Loire *et al.*[4] did choose the b^*c^* plane as scattering plane, and they observed a clear asymmetry between the intensities of unpolarized neutrons scattered at $(0\,1\,q)$ and $(0\,1\,-q)$ caused by J_3 being different from J_5. The branches starting out from zero energy at $(0\,1\,\ell - Q)$ were found to be much more intense than the $(0\,1\,\ell + Q)$ branches [see also the left figure showing $S(0\,1\,q)$ in Fig. 8 below]. This is in agreement with the theoretical predictions, if J_5 is the dominant interplanar interaction, or, more accurately formulated, the theory becomes in accord with these experimental results if the sign of R in Eq. (7) is chosen to be negative, the choice of which is already made with the model parameters introduced by Eq. (22). The experiments of Loire *et al.*[4] were done on a crystal for which the structural chirality was determined to be $\epsilon_T = -1$ from the anomalous part of the x-ray scattering function.[1] This means that the unpolarized neutron experiments of Loire *et al.*[4] show that the strongest interplanar interaction J_5 is, as expected,[1,3] the one determined by the shortest super-superexchange path. The conclusion that $\text{sign}(R) = \epsilon_T$ and, therefore, according to Eq. (8), $\epsilon_H = \epsilon_T\,\epsilon_\gamma$ or $\epsilon_\gamma = \epsilon_H \epsilon_T$ is the same one derived by Marty *et al.*[1] from their unpolarized neutron-diffraction experiments. The elastic and the inelastic unpolarized neutron experiments independently show that the relation $\epsilon_H = \epsilon_T\,\epsilon_\gamma = -\epsilon_T\,\text{sign}(D_c)$ applies, but are unable to decide on the helicity of the magnetic structure ϵ_H and, thereby, on the sign of D_c or the orientation of the ordered spin triangles. The unpolarized neutron scans in the a^*c^* plane should show the similar asymmetry except that the high-intensity branch is the one starting out from $(1\,0\,\ell + Q)$. Preliminary results by Stock *et al.*[11] show a pronounced asymmetry between the scattering at $(1\,0\,\ell + Q)$ and $(1\,0\,\ell - Q)$, but the branch with the largest intensity is the one emerging from $(1\,0\,\ell - Q)$, which indicates that their crystal has $\epsilon_T = +1$, i.e., the opposite structural chirality to that of the crystal investigated by Loire *et al.*[4] The coincidence that the distance between the Fe ions in the triangles is close to $(\sqrt{3}/4)a$ implies that the asymmetry disappears around Bragg points $(h\,k\,\ell)$, when for example $h + k = 2$, as in the case considered in Fig. 5.

IV. HELICALLY POLARIZED SPIN WAVES

Loire *et al.*[4] have performed a series of inelastic scattering experiments in the b^*c^* plane with polarized neutrons. In these experiments, they determined the spin-flip scattering

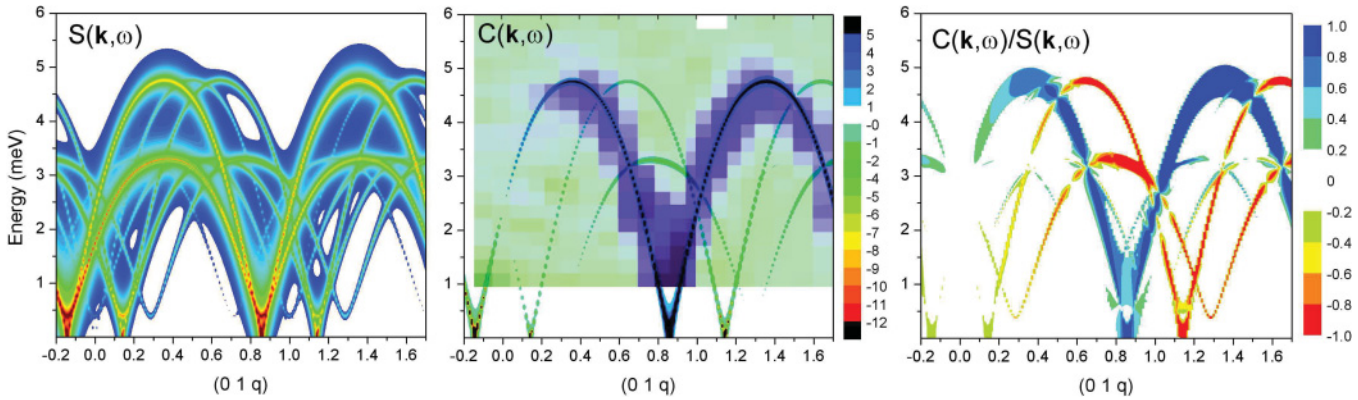

FIG. 8. (Color online) Contour plots of the calculated spin-wave scattering intensities along $\mathbf{k} = (0\,1\,q)$. The left figure shows the logarithmic intensities $S(\mathbf{k},\omega)$ derived for unpolarized neutron scattering. Notice that the intensities of the branches starting out from zero energy at $(0\,1\,\ell - Q)$ are much higher than the intensities of the $(0\,1\,\ell + Q)$ branches. The figure in the middle shows the calculated polarization function $C(\mathbf{k},\omega)$ using a linear scale. The calculated intensities are compared with the experimental results obtained by Loire *et al.* (Ref. 4), which are shown by the green and blue squares lying in the interval between 1 and 6 meV. The figure to the right shows the calculated dynamic scattering ratio $C(\mathbf{k},\omega)/S(\mathbf{k},\omega)$.

intensities $I^{\pm/\mp}$ corresponding to the differential cross sections (within the terminology of Moon, Riste, and Koehler[12])

$$\frac{d\sigma^{\pm/\mp}}{d\Omega} = \sum_{ij} e^{i\mathbf{k}\cdot\mathbf{r}_{ij}}\, p_i p_j^* [\mathbf{S}_{\perp i}\cdot\mathbf{S}_{\perp j} \mp i\hat{\mathbf{z}}\cdot(\mathbf{S}_{\perp i}\times\mathbf{S}_{\perp j})]. \tag{23}$$

In their experiments, Loire *et al.* did choose the neutron-spin polarization vector $\hat{\mathbf{z}}$ to be parallel to the scattering vector $\mathbf{k} = \mathbf{k}_{\text{initial}} - \mathbf{k}_{\text{final}}$, i.e., $\hat{\mathbf{z}} = \mathbf{k}/|\mathbf{k}|$, and extracted the following inelastic scattering functions[4]:

$$S(\mathbf{k},\omega) = \frac{I^{\pm}(\mathbf{k},\omega) + I^{\mp}(\mathbf{k},\omega)}{2},$$
$$C(\mathbf{k},\omega) = \frac{I^{\pm}(\mathbf{k},\omega) - I^{\mp}(\mathbf{k},\omega)}{2}. \tag{24}$$

In the case where the spins of the incident neutrons are polarized parallel to the scattering vector $\mathbf{k}$, $I^{\pm}(\mathbf{k},\omega)$ is the intensity of the scattered neutrons with the opposite polarization. Since $\hat{\mathbf{z}}$ is reversed by definition, when $\mathbf{k}$ is replaced by $-\mathbf{k}$, it is found that $C(\mathbf{k},\omega) = C(-\mathbf{k},\omega)$ as well as $S(\mathbf{k},\omega) = S(-\mathbf{k},\omega)$. The expression given by Eq. (16) in Ref. 6 is straightforwardly generalized so to include $C(\mathbf{k},\omega)$: the products of spin components appearing above in Eq. (23) are translated into the corresponding tensor components of the correlation function in Eq. (16) of Ref. 6, but notice that the sign convention for the wave vectors applied in this reference is the opposite of that used above. For a simple right-handed ($\epsilon_H = +1$) helix with ordering wave vector $Q\mathbf{c}^*$ $(0 < Q < 1/2)$, the elastic response $I^{\mp}$ is nonzero, and $I^{\pm}$ is zero, for the magnetic Bragg peaks at $\mathbf{k} = (0\,0\,|\ell| + Q)$ and $(0\,0\,-|\ell| - Q)$, whereas the opposite is the case for the remaining Bragg points along $\mathbf{c}^*$. The ratio between the static scattering functions $C(\mathbf{k})$ and $S(\mathbf{k})$ for a simple helix with helicity ϵ_H is in general found to be

$$\frac{C(\mathbf{k})}{S(\mathbf{k})} = \frac{2\cos\theta}{1+\cos^2\theta}[\delta(\mathbf{G}-\mathbf{Q}-\mathbf{k}) - \delta(\mathbf{G}+\mathbf{Q}-\mathbf{k})]\,\epsilon_H, \tag{25}$$

where $\cos\theta = \mathbf{k}\cdot\mathbf{Q}/|\mathbf{k}||\mathbf{Q}|$ and $\mathbf{G}$ is a reciprocal lattice vector.

The polarized inelastic neutron-scattering experiments performed by Loire *et al.*[4] on a crystal with $\epsilon_T = -1$ showed that $C(\mathbf{k},\omega)$ is positive and very nearly equal to $S(\mathbf{k},\omega)$ at the lowest energies observed (1 meV) close to the Bragg point at (0 1 6/7), and that this is also the case for the c mode at (0 1 1.3) as shown in Fig. 9. The behavior of $C(\mathbf{k},\omega)$ was measured along $(0\,1\,q)$, and the results shown by Loire *et al.* in their Fig. 3(e) are very similar to the calculated results as indicated by the comparison shown in the middle figure in Fig. 8 (the calculated weak, light-green branches included in this figure were not detectable). The sign of $C(\mathbf{k},\omega)$ determines the sign of the helicity of the helically ordered moments, and, as concluded by Loire *et al.*,[4] their results show that the helicity $\epsilon_H = +1$. This result, in combination with the unpolarized result $\epsilon_T = \text{sign}(R) = -1$ and the maximization of $-J(Q)$ [Eq. (8)], implies that $\epsilon_\gamma = -1$ corresponding to a positive value of D_c.

For a simple helix, the spin-wave theory[13,14] predicts the dynamic ratio between the scattering functions $C(\mathbf{k},\omega)/S(\mathbf{k},\omega)$

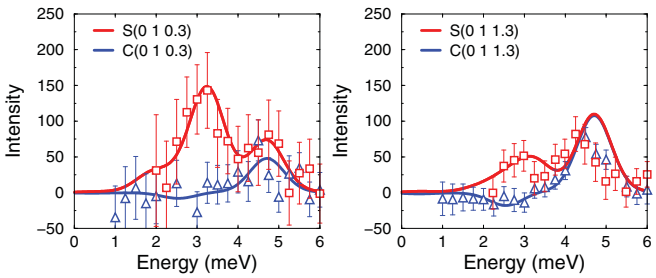

FIG. 9. (Color online) Comparison between theory and experiments for two of the scattering vectors considered in Fig. 8. The experimental results are obtained by Loire *et al.* (Ref. 4) from inelastic scattering of polarized neutrons. The intensity scaling factor and the resolution width are kept constant in all the calculated results.

to be a purely geometric quantity, such as the static one in Eq. (25):

$$\frac{C(\mathbf{k},\omega)}{S(\mathbf{k},\omega)} = \pm\frac{2\cos\theta}{1+\cos^2\theta}\,\epsilon_H\,. \tag{26}$$

This expression applies to the modes emerging from the magnetic Bragg points, which scatter the neutrons via the planar spin components. The sign to be chosen for the $\pm$ sign in front is the same as the sign in front of the corresponding delta function in the magnetic Bragg scattering ratio in Eq. (25), i.e., the $+$ sign applies to the modes starting out from the Bragg points at $\mathbf{G}-\mathbf{Q}$. In contrast to this, the cross section deriving from the c component of the spins is not affected by the helicity, and $C(\mathbf{k},\omega)=0$ for the branches emerging from the nuclear Bragg peaks. With the restriction that we shall only consider spin waves propagating along the c axis, this simple description applies almost unchanged to the present ordered system consisting of three sublattices of coupled helices. $C(\mathbf{k},\omega)=0$ for the c modes emerging from the nuclear Bragg peaks at $\mathbf{G}$ and for the w modes starting out from the magnetic Bragg peaks at $\mathbf{G}\pm\mathbf{Q}$. The c modes detected via the spin components in the ab plane are the branches emerging from the magnetic Bragg points $\mathbf{G}\pm\mathbf{Q}$, and the chiral scattering ratio for these modes is determined by Eq. (26). In principle, the w modes starting out from a nuclear Bragg point or from $\mathbf{G}\pm 2\mathbf{Q}$ should show a dynamic scattering ratio, which is also determined by Eq. (26). However, the $\pm 2\mathbf{Q}$ branches are weak, and the two w modes emerging from the same Bragg point are not easy to separate, and since the chiral scattering ratios have opposite sign for the two branches, they are going to appear like a single mode with a chiral polarization factor close to zero. In the scan along $(0\,0\,q)$ shown in Fig. 7, the upper one of the two nearly degenerate w modes, the $-Q$ branch, has $C(\mathbf{k},\omega)/S(\mathbf{k},\omega)=+1$, whereas $C(\mathbf{k},\omega)/S(\mathbf{k},\omega)=-1$ for the other $+Q$ mode. These results are valid in the case where the spin waves are propagating along the c axis, and they agree in most details with the dynamic scattering ratios calculated numerically using the RPA model. One example is shown in the right of Fig. 8. In principle, the colors in this figure should become more and more blue $[C(\mathbf{k},\omega)/S(\mathbf{k},\omega)=+1]$ or more and more red $[C(\mathbf{k},\omega)/S(\mathbf{k},\omega)=-1]$ for increasing values of q, however, this systematic behavior is going to be disturbed whenever intensities from modes with different helicity factors overlap each other [notice that $|C(\mathbf{k},\omega)/S(\mathbf{k},\omega)|$ is predicted to be 0.967, nearly 1, already at $q=6/7$]. The inelastic cross section is readily calculated numerically in the general case, but the result becomes less transparent due to the complication that the c and w modes are coupled whenever the propagation vector has a nonzero component in the ab plane.

V. CONCLUSION

The intratriangular interaction $J_1>0$ is the dominant cause for the relatively strong frustration shown by the present spin system, and it is important to account for this interaction primary to the interactions between the Fe triangles. The MF approximation, when applied to the trimerized clusters, leads to a much improved description of the system in comparison with the single-spin approximation. The susceptibility just above T_N is being reduced by 15%, the transition temperature by 50%, and the paramagnetic Curie temperature is derived to be -190 K, not -142 K as predicted by the simple theory. The analysis of the spin waves in terms of the five exchange constants, plus the DM anisotropy, leaves one exchange constant as a nearly free variable. In the present analysis, this degree of freedom has been fixed by a fitting to the susceptibility implying that a precise description of the ground state is essential for a trustworthy determination of the exchange constants. The present model accounts very well for the susceptibility, whereas the use of, for instance, the exchange parameters proposed by Loire *et al.*[4] leads to values for the susceptibility, which are about 25% larger than the experimental ones (40% in the single-spin MF approximation) at temperatures close to T_N. The MF-cluster calculation also predicts a quantum reduction of the ordered moment, from 5 to 4.7 μ_B. This reduction is less pronounced than the one derived from experiments, as the value of the ordered moment determined from neutron-diffraction experiments at 2 K by Marty *et al.*[1] was found to be as small as about 4 μ_B.

Although the trimerized states of the Fe spin triangles deviate substantially from that determined by fully polarized spins, the linear spin-wave theory [Eqs. (18) and (19)] works surprisingly well. The energies predicted by the linear theory (the dashed lines in Fig. 4) only differ by about 5% at maximum from that predicted by the more accurate numerical RPA calculations. This effectiveness of the boson representation obtained by, for instance, the Holstein-Primakoff transformation is of similar significance for the analysis of an anisotropic ferromagnet such as terbium metal discussed at length in Refs. 5 and 15. A comparison with this theory, which utilizes systematically $1/S$ as an expansion parameter, suggests the corrections to the present linear theory to be of order $(\lambda/2S)^2$ rather than λ^2. The particular model derived by Loire *et al.*[4] based on the linear spin-wave theory is questioned, but their theoretical results are found to agree closely with the predictions of the present theory. Their characterization of the different spin-wave modes may be imprecise, but their main conclusions are the same as derived here. In the crystal they investigated, the crystallographic chirality is $\epsilon_T=-1$, the ordered moments in the triangles have the orientation specified by $\epsilon_\gamma=-1$, and the spiraling ordered moments along a line parallel to the c axis are making a right-handed helix corresponding to $\epsilon_H=+1$.

The mirroring of the present system with respect to, for instance, the ac plane through $\mathbf{S}_1$ would change the structural chirality ϵ_T from -1 to $+1$, and the helicity ϵ_H from $+1$ to -1, whereas the sign of $D_c(>0)$ and $\epsilon_\gamma=-1$ would remain unchanged. The choice between the two possible orientations of the ordered spin triangles is determined by the local surroundings, not by the structural chirality. By definition, chirality should be invariant with respect to time reversal but have odd parity with respect to inversion.[16] Based on this definition, the orientation of the spin triangles denoted by ϵ_γ can not be characterized as a chiral property.

To summarize: The asymmetry between the inelastic intensities of magnetic scattered unpolarized neutrons at $(0\,1\,\ell-q)$ and $(0\,1\,\ell+q)$ or at $(1\,0\,\ell-q)$ and $(1\,0\,\ell+q)$, as observed, respectively, by Loire *et al.*[4] and by Stock *et al.*,[11] is alone a consequence of the structural chirality. ϵ_T is equal to -1

in the crystal studied by Loire *et al*., whereas $\epsilon_T = +1$ is the preliminary result for the crystal investigated by Stock *et al*. The DM anisotropy term D_c in Eq. (2), due to the spin-orbit interaction, couples chirality in spin space to the crystallographic chirality $\epsilon_H = \epsilon_\gamma \epsilon_T$. The sign of the DM anisotropy determines the choice between the two possible orientations of the ordered moments in the Fe triangles, and it is found that $\epsilon_\gamma = -\text{sign}(D_c) = -1$. The combination of an enantiopure crystal and a nonzero DM anisotropy implies that the system only contains ordered moments with a single sense of helicity, and that $\epsilon_H = -\epsilon_T$ in this system where D_c is positive. The dynamics of the present system is unique, not because the spin waves have chiral properties, but because the presence of only one domain of helicity has made it possible to observe this intrinsic dynamic property. It may be concluded that the three different modes of spin waves propagating along the c axis in the $Ba_3NbFe_3Si_2O_{14}$ crystal investigated by Loire *et al*.[4] should all possess, depending on their effective propagation vector $\mathbf{q} = \mathbf{k} - \mathbf{G}$, the same or the opposite sense of helicity as the ordered structure. The observed behavior of the c mode is in agreement with this conclusion, whereas the near degeneracy of the w modes starting out from the nuclear Bragg points prevents an experimental determination of the chiral properties of these modes.

ACKNOWLEDGMENTS

D. F. McMorrow is gratefully acknowledged for stimulating discussions and for providing me with the neutron-scattering results obtained by Stock *et al*.[3,11] prior to publication. I also want to thank S. W. Lovesey for making me aware of the precise definition of "chirality."

[1] K. Marty, V. Simonet, E. Ressouche, R. Ballou, P. Lejay, and P. Bordet, Phys. Rev. Lett. **101**, 247201 (2008).

[2] K. Marty, V. Simonet, P. Bordet, R. Ballou, P. Lejay, O. Isnard, E. Ressouche, F. Bourdarot, and P. Bonville, J. Magn. Magn. Mater. **321**, 1778 (2009).

[3] C. Stock, L. C. Chapon, A. Schneidewind, Y. Su, P. G. Radaelli, D. F. McMorrow, A. Bombardi, N. Lee, and S.-W. Cheong, Phys. Rev. B **83**, 104426 (2011).

[4] M. Loire, V. Simonet, S. Petit, K. Marty, P. Bordet, P. Lejay, J. Ollivier, M. Enderle, P. Steffens, E. Ressouche, A. Zorko, and R. Ballou, Phys. Rev. Lett. **106**, 207201 (2011).

[5] J. Jensen and A. R. Mackintosh, *Rare Earth Magnetism: Structures and Excitations* (Oxford University Press, Oxford, 1991); [http://www.nbi.ku.dk/page40667.htm].

[6] J. Jensen, Phys. Rev. B **79**, 014406 (2009).

[7] T. Moriya, Phys. Rev. **120**, 91 (1960).

[8] K. Marty, P. Bordet, V. Simonet, M. Loire, R. Ballou, C. Darie, J. Kljun, P. Bonville, O. Isnard, P. Lejay, B. Zawilski, and C. Simon, Phys. Rev. B **81**, 054416 (2010).

[9] A. P. Ramirez, Annu. Rev. Mater. Sci. **24**, 453 (1994).

[10] M. Janoschek, F. Bernlochner, S. Dunsiger, C. Pfleiderer, P. Böni, B. Roessli, P. Link, and A. Rosch, Phys. Rev. B **81**, 214436 (2010).

[11] C. Stock, L. C. Chapon, A. Schneidewind, Y. Su, P. G. Radaelli, D. F. McMorrow, A. Bombardi, N. Lee, and S.-W. Cheong (private communication).

[12] R. M. Moon, T. Riste, and W. C. Koehler, Phys. Rev. **181**, 920 (1969).

[13] V. G. Bar'yakhtar and S. V. Maleev, Sov. Phys. Solid State **5**, 858 (1963) [Fiz. Tverd. Tela **5**, 1175 (1963)].

[14] S. W. Lovesey and G. I. Watson, J. Phys. Condens. Matter **10**, 6761 (1998).

[15] J. Jensen, J. Phys. C: Solid State Phys. **8**, 2769 (1975).

[16] H. D. Flack, Helv. Phys. Acta **86**, 905 (2003).